# Higher-Order Topological Peierls Insulator in a Two-Dimensional Atom-Cavity System

Joana Fraxanet,[1,*] Alexandre Dauphin,[1] Maciej Lewenstein,[1,2] Luca Barbiero,[3] and Daniel González-Cuadra[4,5,†]
[1]ICFO—Institut de Ciències Fotòniques, The Barcelona Institute of Science and Technology, 08860 Castelldefels (Barcelona), Spain
[2]ICREA, Passeig de Lluís Companys 23, ES-08010 Barcelona, Spain
[3]Institute for Condensed Matter Physics and Complex Systems, DISAT, Politecnico di Torino, I-10129 Torino, Italy
[4]Institute for Theoretical Physics, University of Innsbruck, 6020 Innsbruck, Austria
[5]Institute for Quantum Optics and Quantum Information of the Austrian Academy of Sciences, 6020 Innsbruck, Austria

(Received 22 May 2023; accepted 27 November 2023; published 27 December 2023)

In this work, we investigate a two-dimensional system of ultracold bosonic atoms inside an optical cavity, and show how photon-mediated interactions give rise to a plaquette-ordered bond pattern in the atomic ground state. The latter corresponds to a 2D Peierls transition, generalizing the spontaneous bond dimerization driven by phonon-electron interactions in the 1D Su-Schrieffer-Heeger (SSH) model. Here the bosonic nature of the atoms plays a crucial role to generate the phase, as similar generalizations with fermionic matter do not lead to a plaquette structure. Similar to the SSH model, we show how this pattern opens a nontrivial topological gap in 2D, resulting in a higher-order topological phase hosting corner states, that we characterize by means of a many-body topological invariant and through its entanglement structure. Finally, we demonstrate how this higher-order topological Peierls insulator can be readily prepared in atomic experiments through adiabatic protocols. Our work thus shows how atomic quantum simulators can be harnessed to investigate novel strongly correlated topological phenomena beyond those observed in natural materials.

DOI: 10.1103/PhysRevLett.131.263001

*Introduction.*—In the last decades, topology has reached a central role in the description and classification of phases of matter [1]. Contrary to the standard Landau paradigm [2], topological phases are not distinguished by different spontaneous symmetry-breaking (SSB) patterns, but rather by different nonlocal topological invariants [3,4]. Nontrivial topology can manifest in the presence of conducting edge states in bulk insulators [5–7], quantized conductances [8–11], or fractional charges [12–14], which in the case of symmetry-protected topological (SPT) phases are robust against perturbations that do not break certain protecting symmetries [15]. Recently, this class has been enlarged to include higher-order SPT (HOSPT) phases [16,17], protected by crystalline symmetries and hosting edge states of codimension larger than one, such as corner states in 2D [18,19]. Despite recent progress in the study of interacting HOSPT phases [20–36], a full classification is still lacking.

One of the earliest examples of a SPT phase is found in the Su-Schrieffer-Heeger (SSH) model for polyacetylene [37]. In this 1D chain, interactions between electrons and phonons induce a Peierls instability [38], giving rise to a $\mathbb{Z}_2$ SSB characterized by a dimerized bond pattern, resulting in a topologically nontrivial bulk protected by a chiral symmetry [39]. In this case, the interplay between symmetry breaking and symmetry protection gives rise to delocalized fractional charges [40], absent in the noninteracting case [3,4].

As shown by Benalcazar, Bernevig, and Hughes (BBH) [16,17], a 2D fermionic system with dimerized bonds in the $x$ and $y$ directions can host a HOSPT phase, but only in the presence of a nonzero flux. The latter is not generated by generalizations of the SSH model to 2D, since the required symmetry-broken pattern is not achieved spontaneously, as shown by recent Monte Carlo studies [41].

The situation is different for the bosonic BBH model [21,27], where a topological gap appears without any flux. A natural question is whether the corresponding HOSPT phase can emerge through a SSB process from a symmetric bosonic Hamiltonian, where, similarly to the 1D case [42], the interplay between SSB and symmetry protection could be further explored. Contrary to solid-state materials, ultracold atoms in optical lattices allow us to investigate strongly correlated bosonic matter in highly controllable experiments [43–45]. Although optical lattices are static, the role of phonons can be emulated using a second atomic species [46] or with a cavity [47,48]. In 1D, these synthetic phonons drive solid-state-like phenomena, including topological Peierls insulators [42,49–59] and fractional charges [60–62], also predicted in the presence of dipolar interactions [63].

In this work, we extend these results to 2D by considering a system of ultracold bosonic atoms coupled to a cavity, a setup that has been previously employed to prepare quantum phases such as supersolids or charge density waves [64,65]. We show how, by modifying the

 

phase of the cavity mode, a plaquette-ordered structure with dimerization both in the $x$ and $y$ directions appears, driven by photon-mediated interactions. This symmetry-broken pattern is indeed the same as the one required in the bosonic BBH model, but here it emerges spontaneously through a bosonic Peierls transition. Contrary to the 1D case [42], where fermions and (hardcore) bosons are essentially equivalent, our results show how bosonic particles in 2D can self-organize in an intrinsically new phase of matter, that cannot be generated with a symmetric fermion-phonon model [41]. We confirm the topological nature of this phase, that we denote higher-order topological Peierls insulator (HOTPI), using a many-body topological invariant and through its entanglement structure. Finally, we propose and benchmark a quantum simulation protocol to adiabatically prepare this phase in current atomic experiments.

*Bose-Hubbard model with cavity-mediated correlated tunneling.*—We consider a system of ultracold bosonic atoms trapped in the lowest band of a $L \times L$ square optical lattice. The atoms are coupled to two cavity modes created by two cavities aligned along the $x$ and $y$ directions, together with a laser pump with a standing wave structure in the $z$ direction [Fig. 1(a)]. In the basis of localized Wannier functions, the system is described by the following Hamiltonian [66]:

$$H = -t\sum_{\langle i,j\rangle}(b_i^\dagger b_j + \text{H.c.}) + \frac{U}{2}\sum_j n_j(n_j-1) - \Delta_c \sum_{\mu\in\{x,y\}} a_\mu^\dagger a_\mu + g\sum_{\mu\in\{x,y\}}(a_\mu + a_\mu^\dagger)B_\mu, \quad (1)$$

with $B_\mu = \sum_i (-1)^{i+1}(b_i^\dagger b_{i+\hat{\mu}} + \text{H.c.})$, where $\hat{\mu}$ denotes the unit translation in the $\hat{x}/\hat{y}$ direction. Here, $b_i^\dagger/b_i$ denotes the bosonic creation(annihilation) atomic operator at site $i$, and $a_\mu^\dagger/a_\mu$ is the creation(annihilation) photon operator for the $x/y$ cavity mode. The parameters $t$ and $U$ correspond to the standard nearest-neighbor (NN) tunneling and Hubbard onsite interactions [67], respectively, and $\Delta_c$ is the cavity-pump detuning [66]. Finally, $g$ characterizes the atom-cavity interactions, where, differently to previous experiments [64,65], the latter is not coupled to the density but to the staggered tunneling $B_\mu$. This leads to a mediated tunneling term for each cavity separately, since the scattering between the cavities can be neglected [68]. Similarly to the 1D case [42], this is achieved by considering a relative phase $\phi = \pi/2$ between the cavity modes and the optical lattice [Fig. 1(b)] (see [68]), guaranteeing momentum conservation in the scattering process.

The atom-cavity Hamiltonian is invariant under $\mathbb{Z}_2 \times \mathbb{Z}_2$ transformations, each $\mathbb{Z}_2$ symmetry corresponding to a one-site translation of the atoms in the direction $\mu$ together with the transformation $a_\mu \to -a_\mu$. We anticipate that the HOTPI will be driven by the spontaneous breaking of this symmetry. Before analyzing the phase diagram, we adiabatically

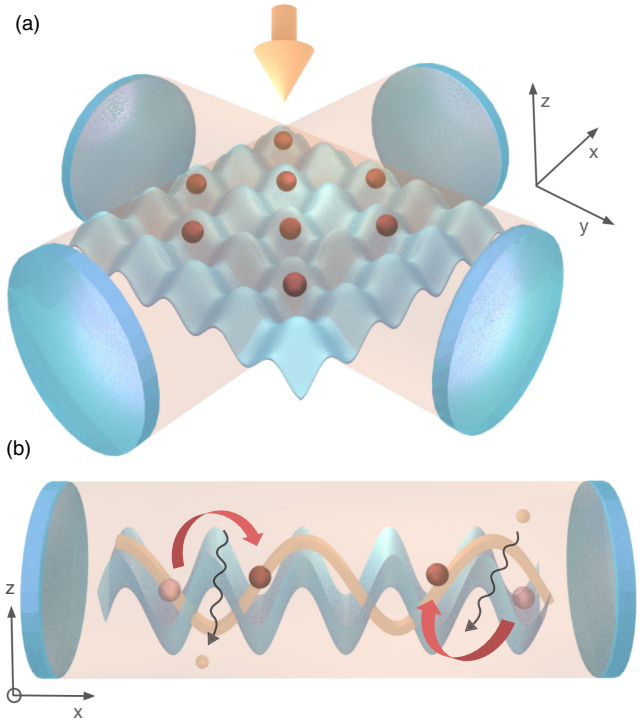


FIG. 1. Atom-cavity experimental setup: (a) Ultracold bosonic atoms are trapped in the lowest band of a 2D optical lattice. The atoms are coupled to two cavity modes created by two optical cavities aligned in the $x$ and $y$ directions, and to a laser pump aligned in the $z$ direction. (b) In each direction, the relative phase between the optical lattice (blue) and the cavity mode (yellow) is chosen such that the nodes of the latter coincide with the sites of the lattice. In this configuration, the effective Hamiltonian describing the atom-cavity system contains correlated-tunneling terms (red arrows), where atoms can tunnel between NN sites by absorbing or emitting a photon (white sphere) from the cavity (curly line).

eliminate the cavity modes in the presence of a large cavity decay rate [66], resulting in the limit of large detuning $\Delta_c$ in the following expression (see [68]):

$$H_{\text{eff}} = -t\sum_{\langle i,j\rangle}(b_i^\dagger b_j + \text{H.c.}) + \frac{U}{2}\sum_{i=j}^{N} n_j(n_j-1) + \frac{U_c}{L^2}\sum_\mu B_\mu^2, \quad (2)$$

with $U_c = g^2L^2/\Delta_c$. The last term in Eq. (2) accounts for the cavity-mediated all-to-all interactions arising from the correlated tunneling terms in Eq. (1). The latter differs from the cavity-mediated density-density interaction considered in Refs. [64,65] for $\phi = 0$, giving rise to a charge density wave and a supersolid phase. As we show below, a HOTPI can be obtained with the same experimental setup by choosing instead $\phi = \pi/2$.

*Bosonic Peierls transition in 2D.*—We study the phase diagram of the effective Hamiltonian (2) in the hardcore boson limit ($U \gg t, U_c$) as a function of

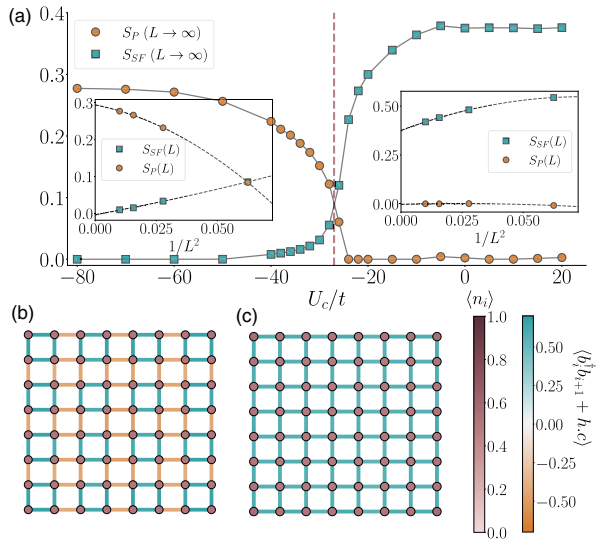


FIG. 2. Phase diagram: (a) SF ($S_{\mathrm{SF}}$) and plaquette ($S_{\mathrm{P}}$) order parameters in the thermodynamic limit by a finite-size scaling, indicating the presence of a plaquette-ordered phase for $U_c/t \lessapprox -27$, and a SF for $U_c/t \gtrapprox -27$. The insets show the finite-size scaling at $U_c/t = -80$ (left) and $U_c/t = 10$ (right) for system sizes $L \times L$, with $L \in \{4, 6, 8, 10\}$. (b) and (c) show the real-space configuration of the plaquettes at $U_c/t = -80$ and the SF at $U_c/t = 30$, respectively. The color of the lattice sites and bonds denotes the expectation value of the onsite occupation $\langle n_i\rangle$ and the NN tunneling $\langle b_i^\dagger b_j^\dagger + \mathrm{H.c.}\rangle$, respectively.

the cavity-mediated interaction strength $U_c$. In the following, and unless stated otherwise, we fix the atomic density to half-filling, $N = L^2/2$, and consider open boundary conditions. The ground state is obtained using a density-matrix renormalization group (DMRG) algorithm [69] based on matrix product states [70], where we consider bond dimensions up to $\chi = 1000$.

As we show in Fig. 2(a), for positive or small negative values of $U_c$, the system is in a superfluid (SF) with off-diagonal long-range order, characterized by a finite value of the single-particle momentum distribution $S(\mathbf{q})$ at $\mathbf{q} = (0,0)$, $S_{\mathrm{SF}} \equiv S(0)$, with

$$S(\vec{q}) = \frac{1}{L^2}\sum_{i,j}\langle b_i^\dagger b_j + \mathrm{H.c.}\rangle e^{i\mathbf{q}(\mathbf{r_i}-\mathbf{r}_j)}, \tag{3}$$

where the indices in the sum run over every pair of sites. For $U_c/t \lessapprox -27$, the cavity-mediated interactions induce a plaquette-ordered phase [71,72] through a spontaneous breaking of the $\mathbb{Z}_2 \times \mathbb{Z}_2$ symmetry. The latter is characterized by a finite value of the plaquette structure factor [73],

$$S_{\mathrm{P}} = \frac{1}{(L-1)L-3}\sum_{\langle k,l\rangle}\epsilon(k,l) \times [\langle b_i^\dagger b_j b_k^\dagger b_l + \mathrm{H.c.}\rangle - \langle (b_i^\dagger b_j + \mathrm{H.c.})^2\rangle], \tag{4}$$

where the sum $\langle k,l\rangle$ runs over NN pairs, $\langle i,j\rangle$ is a fixed bond in the middle of the lattice, and the form factor $\epsilon(k,l)$ is defined as in Ref. [73].

Figure 2(b) shows the real-space configuration of the plaquette-ordered phase, where the expectation value of the NN bosonic tunneling reveals a bond dimerization both in the $x$ and $y$ directions, contrary to the translational invariant SF case [Fig. 2(c)]. Figure 2(a) shows the finite-size scaling for the ground state values of the order parameters in each phase, demonstrating how $S_{\mathrm{P}}$ ($S_{\mathrm{SF}}$) goes to zero (finite value) for the SF phase in the thermodynamic limit ($L \to \infty$), and vice versa for the plaquette-ordered phase. Finally, we show the extrapolated values as a function of $U_c/t$, consistent with a 2D bosonic Peierls transition between these two phases at $U_c/t \approx -27$. The $\mathbb{Z}_2 \times \mathbb{Z}_2$ SSB is driven by the competition between the usual tunneling and the atom-photon interactions, resulting in a plaquette pattern for the tunneling amplitudes. This is a generalization of the Peierls transition driven by electron-phonon interactions in the SSH model [37]. In this case, the bosonic nature of the atoms, and an equal coupling to the cavities [65], are crucial to obtain this phase, absent in the fermionic 2D SSH model, where only one $\mathbb{Z}_2$ symmetry is broken [41]. Since this emergent plaquette structure corresponds to the one imposed externally in the bosonic BBH model [21,27], it is therefore natural to ask whether this phase is topologically nontrivial.

*Higher-order topological Peierls insulator.*—We analyze now the topological properties of the plaquette-ordered phase, showing that it corresponds to a HOSPT phase. Similarly to the bosonic BBH model [21,27], the latter is protected by a $U(1) \times C_4$ symmetry, where $U(1)$ is the particle number conservation and $C_4$ is the lattice rotational symmetry, preserved here in the plaquette phase. We confirm the topological nature of the phase through its entanglement spectrum (ES) structure [74] and a many-body topological invariant [75].

We start by studying the entanglement spectrum along different bipartitions. As a result of the SSB, the plaquette-ordered phase is fourfold degenerate, connected by one-site translations along the $x$ and $y$ directions. Finite-size effects introduce energy splittings in the ground-state manifold, vanishing exponentially with the system size. Although the lowest-energy state for finite sizes is the one with positive values of $\langle b_i^\dagger b_j + \mathrm{H.c.}\rangle$ around the corners [Fig. 2(b)], we stress that the topological configuration, presenting negative values [Fig. 3(b)], can be adiabatically prepared as a long-lived metastable state, as we show below.

Figure 3(a) shows the ES for the ground state in the plaquette-ordered phase at different bipartitions. In general, the ground-state wave function can be written as $|\psi_{\mathrm{GS}}\rangle = \sum_n e^{-\epsilon_n/2}|\psi_n\rangle_A \otimes |\psi_n\rangle_B$, where $A$ and $B$ are complementary subsets of lattice sites, and $\epsilon_n$ is the corresponding ES associated to that bipartition. For HOSPT phases, bipartitions that create virtual corners lead to even degenerate

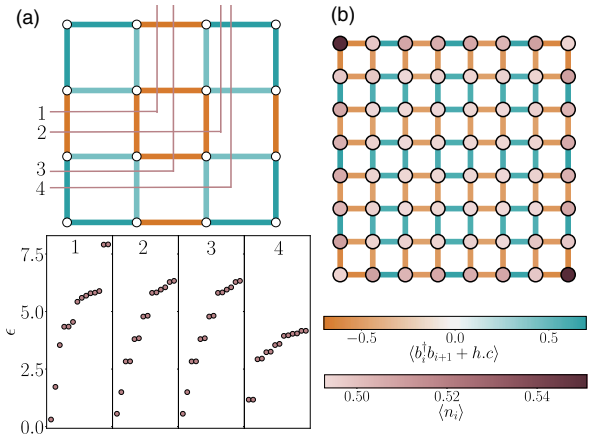


FIG. 3. ES structure and corner states. (a) Lower eigenvalues of the ES for the bipartitions indicated in the Figs. 1–4. We consider the ground state of a system with size $L = 4$ at $U_c/t = -40$ (within the plaquette-ordered phase). (b) Real-space bond pattern and local occupation for the topological configuration at $U_c/t = -100$, for a system with $L = 10$. Because of the quasidegeneracy of the ground state, this state is not the lowest energy state of the system, but it is instead metastable.

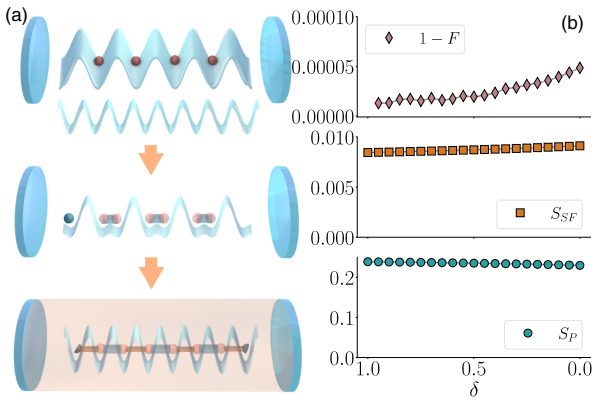


FIG. 4. Adiabatic preparation of the HOTPI. Sketch of the three main steps of the preparation scheme (a), starting with a deep lattice with wavelength $\lambda$, adding a second optical lattice with wavelength $\lambda/2$, and turning on the cavity and adiabatically eliminating the first lattice. (b) Infidelity $1 - F$ (where $F = |\langle \psi_{i-1} | \psi_i \rangle|$ is the quantum fidelity at each step), superfluid ($S_{\mathrm{SF}}$), and plaquette ($S_{\mathrm{P}}$) order parameters for a finite system with $L^2 = 64$, along the third step of the experimental protocol, where the two-dimensional dimerization $\delta$ is taken from 1 to 0 (see main text). The results are obtained for $U_c/t = -100$.

spectra [74]. In our case, and similarly to the bosonic BBH model, the broken $\mathbb{Z}_2 \times \mathbb{Z}_2$ symmetry allows for four inequivalent bipartitions. Only the one that creates a virtual corner surrounded by weak bonds, similar to the virtual edges in the 1D case [50], has a degenerate ES [Fig. 3(a)].

The ES is a bulk quantity that provides information on the topological nature of the phase, but also indicates the possibility of finding localized states in a physical corner for finite systems. Such corner states are fractionalized charges which correspond to an accumulation of a charge of $Q = 1/2$ [27] with respect to the average bulk filling $n = 0.5$. Even if there is no bulk-boundary correspondence for a HOSPT phase protected by the $U(1) \times C_4$, as indicated in [21,27], or in the presence of global interactions [76], we find a signature of corner states in the topological configuration, as depicted in Fig. 3(b). The corner states are not necessarily located in the middle of the gap, and their localization length can be quite large if they are close to bulk bands, as it appears to be the case here given the small extra atomic occupation with respect to half-filling. A more in-depth characterization requires, therefore, the study of larger system sizes.

We further confirm the topological nature of the plaquette-ordered phase using a many-body topological invariant. We calculate a many-body Berry phase $\gamma$ by introducing a local flux through the central plaquette to the Hamiltonian, as described in Ref. [75], and computing the discretized Wilson loop as we vary the flux along a close path $C$ in parameter space [77]. The Berry phase is approximated by $\gamma_C^m = \mathrm{Arg} \prod_{i=0}^{m-1} \langle \hat{\psi}_i | \hat{\psi}_{i+1} \rangle$, where $|\psi_i\rangle$ is the ground state for a given flux in the discretized loop of $m$ points. The Berry phase, independent of the path, is recovered in the limit of large $m$. We compute this quantity for a system with $L = 10$ and obtain the values $\gamma_C = 4 \times 10^{-5}$ and $\gamma_C = 0.9995 \pmod{2\pi}$ for the SF and plaquette-ordered phases, respectively, confirming the topological nature of the latter. Contrary to the protection of the corner states described above, the topological invariant remains quantized in the presence of global interactions, demonstrating the robustness of the phase.

*Experimental realization.*—We introduce now a protocol to prepare the HOTPI experimentally [Fig. 4(a)]. To prepare the phase adiabatically, we need to break the $\mathbb{Z}_2 \times \mathbb{Z}_2$ symmetry explicitly to avoid closing the gap at the transition. Imposing the appropriate double-well structure for the starting point allows us to select the topological configuration [Fig. 3(b)] among the quasidegenerate ground-state manifold. Even if for finite system sizes this configuration has a slightly higher energy than the others, they are separated by energy barriers that diverge with the system size. As a consequence, during the adiabatic preparation, we are guaranteed to stay in the metastable topological symmetry sector, because shifting to the trivial configuration would require a global $\mathbb{Z}_2 \times \mathbb{Z}_2$ perturbation, which has an exponentially small probability.

We start with a Mott insulator with unit filling in a square optical lattice with wavelength $\lambda$ in each direction, as routinely prepared in ultracold atomic experiments. Following Ref. [78], we then introduce a second optical lattice with wavelength $\lambda/2$, creating a superlattice of double wells with weak bonds connecting the corners. The latter imprints the plaquette structure in the bosonic tunneling and breaks the $\mathbb{Z}_2 \times \mathbb{Z}_2$ symmetry explicitly.

At this point, the atomic Hamiltonian corresponds to the bosonic BBH model in the limit of zero interwell tunneling [27]. Explicitly,

$$H(\delta) = H_{\text{eff}}(U_c = 0) + \delta \sum_{i,\mu} (-1)^{s_i} (b_i^\dagger b_{i+\hat{\mu}} + \text{H.c.}) \quad (5)$$

for the case positive $\delta = 1$, where $s_i = i_0 + i_1$ and $i = (i_0, i_1)$. We now turn on the cavity and tune the coupling $U_c$ to the desired value. By slowly decreasing the intensity of the original $\lambda$-wavelength lattice we take $\delta$ to zero, ending up with the atom-cavity Hamiltonian in Eq. (2).

The protocol is adiabatic as the gap remains open along the path in parameter space. This is shown in Fig. 4(b), where we compute the ground-state infidelity after taking infinitesimal parameter changes along the path by running the DMRG algorithm at each $\delta$ step [79]. Although we did not check the timescales involved in the state preparation, this can be made faster by increasing the dimerization $\delta$, which increases the system's gap. In Fig. 4(b), we also show how $S_{\text{P}}$ and $S_{\text{SF}}$ for a finite size system are consistent with a state in the HOTPI.

Regarding the detection of the HOTPI, the self-organized atomic structure is directly related to the presence of a coherent cavity field, which can be directly measured experimentally [65], and the real-space structure can be observed using a quantum gas microscope [80,81]. Finally, the nontrivial topological nature of the phase can be revealed by measuring the entanglement spectrum [82,83].

*Conclusions and outlook.*—We showed how photon-mediated interactions in a 2D bosonic system can give rise to a HOTPI. The latter can be prepared experimentally using ultracold bosonic atoms in optical lattices, coupled to two perpendicular cavity modes. The cavity-mediated all-to-all atomic interactions drive a Peierls transition, giving rise to a plaquette-ordered phase if the relative phases between the lattice and the cavity modes are properly chosen. Finally, we demonstrated the topological nature of the phase and proposed an adiabatic protocol to prepare it in current atomic experiments. We note that the effect of dissipation in the topology of the full atom-cavity system could be investigated beyond the effective description, which we leave for future studies. Moreover, one should also take into account the inhomogeneities of the trapping potential, which might affect the stability of the plaquette-ordered phase. An alternative is to consider the combination of box traps and optical lattices as in [84], which are promising for the realization of topological phases. In the future, it would be interesting to extend the setup and include multimode cavities, allowing atom-photon topological defects that would generalize the topological solitons and fractionalized quasiparticles found in the SSH model to 2D [37]. Moreover, by exploring the regime of softcore bosons, we expect to find plaquette-ordered supersolid phases, similar to the density-ordered supersolids found in Refs. [64,65].

We thank P. Stammer for discussion. ICFO group acknowledges support from: ERC AdG NOQIA; Ministerio de Ciencia y Innovacion y Agencia Estatal de Investigaciones (PGC2018-0910.13039/501100011033, CEX2019-000910-S/10.13039/501100011033, Plan National FIDEUA PID2019-106901GB-I00, FPI; MICIIN with funding from European Union NextGenerationEU (PRTR-C17.I1): QUANTERA MAQS PCI2019-111828-2); MCIN/AEI/10.13039/501100011033 and by the "European Union NextGeneration EU/PRTR" QUANTERA DYNAMITE PCI2022-132919 within the QuantERA II Programme that has received funding from the European Union's Horizon 2020 research and innovation programme under Grant Agreement No. 101017733Proyectos de I + D + I "Retos Colaboración" QUSPIN RTC2019-007196-7); Fundació Cellex; Fundació Mir-Puig; Generalitat de Catalunya (European Social Fund FEDER and CERCA program, AGAUR Grant No. 2021 SGR 01452, QuantumCAT\U16-011424, co-funded by ERDF Operational Program of Catalonia 2014-2020); EU (PASQuanS2.1, 101113690); EU Horizon 2020 FET-OPEN OPTOlogic (Grant No. 899794); EU Horizon Europe Program (Grant Agreement 101080086—NeQST), National Science Centre, Poland (Symfonia Grant No. 2016/20/W/ST4/00314); ICFO Internal "QuantumGaudi" project; European Union's Horizon 2020 research and innovation program under the Marie-Skłodowska-Curie grant agreement No. 101029393 (STREDCH) and No 847648 ("La Caixa" Junior Leaders fellowships ID100010434: LCF/BQ/PI19/11690013, LCF/BQ/PI20/11760031, LCF/BQ/PR20/11770012, LCF/BQ/PR21/11840013). D. G.-C. is supported by the Simons Collaboration on Ultra-Quantum Matter, which is a grant from the Simons Foundation (651440, P. Z.). The authors thankfully acknowledge the computer resources at MareNostrum and the technical support provided by Barcelona Supercomputing Center (FI-2022-1-0042, FI-2022-3-0039, FI-2023-1-0013). L. B. acknowledges funding from Politecnico di Torino, starting package Grant No. 54 RSG21BL01 and from the Italian MUR (PRIN DiQut Grant No. 2022523NA7).

*joana.fraxanet@icfo.eu
†daniel.gonzalez-cuadra@uibk.ac.at

[1] J. E. Moore, Nature (London) **464**, 194 (2010).
[2] L. D. Landau, Zh. Eksp. Teor. Fiz. **7**, 19 (1937).
[3] M. Z. Hasan and C. L. Kane, Rev. Mod. Phys. **82**, 3045 (2010).
[4] X.-L. Qi and S.-C. Zhang, Rev. Mod. Phys. **83**, 1057 (2011).
[5] A. H. MacDonald, Phys. Rev. Lett. **64**, 220 (1990).
[6] Y. Hatsugai, Phys. Rev. Lett. **71**, 3697 (1993).
[7] S. Ryu and Y. Hatsugai, Phys. Rev. Lett. **89**, 077002 (2002).

[8] K. v. Klitzing, G. Dorda, and M. Pepper, Phys. Rev. Lett. **45**, 494 (1980).
[9] R. B. Laughlin, Phys. Rev. B **23**, 5632 (1981).
[10] D. J. Thouless, M. Kohmoto, M. P. Nightingale, and M. den Nijs, Phys. Rev. Lett. **49**, 405 (1982).
[11] N. Read and G. Moore, Prog. Theor. Phys. Suppl. **107**, 157 (1992).
[12] D. C. Tsui, H. L. Stormer, and A. C. Gossard, Phys. Rev. Lett. **48**, 1559 (1982).
[13] R. B. Laughlin, Phys. Rev. Lett. **50**, 1395 (1983).
[14] W. P. Su and J. R. Schrieffer, Phys. Rev. Lett. **46**, 738 (1981).
[15] C.-K. Chiu, J. C. Y. Teo, A. P. Schnyder, and S. Ryu, Rev. Mod. Phys. **88**, 035005 (2016).
[16] W. A. Benalcazar, B. A. Bernevig, and T. L. Hughes, Science **357**, 61 (2017).
[17] W. A. Benalcazar, B. A. Bernevig, and T. L. Hughes, Phys. Rev. B **96**, 245115 (2017).
[18] F. Schindler, A. M. Cook, M. G. Vergniory, Z. Wang, S. S. P. Parkin, B. A. Bernevig, and T. Neupert, Sci. Adv. **4**, eaat0346 (2018).
[19] E. Khalaf, Phys. Rev. B **97**, 205136 (2018).
[20] Y. You, T. Devakul, F. J. Burnell, and T. Neupert, Phys. Rev. B **98**, 235102 (2018).
[21] O. Dubinkin and T. L. Hughes, Phys. Rev. B **99**, 235132 (2019).
[22] K. Kudo, T. Yoshida, and Y. Hatsugai, Phys. Rev. Lett. **123**, 196402 (2019).
[23] K. Laubscher, D. Loss, and J. Klinovaja, Phys. Rev. Res. **1**, 032017(R) (2019).
[24] K. Laubscher, D. Loss, and J. Klinovaja, Phys. Rev. Res. **2**, 013330 (2020).
[25] A. Sil and A. K. Ghosh, J. Phys. Condens. Matter **32**, 205601 (2020).
[26] A. Rasmussen and Y.-M. Lu, Phys. Rev. B **101**, 085137 (2020).
[27] J. Bibo, I. Lovas, Y. You, F. Grusdt, and F. Pollmann, Phys. Rev. B **102**, 041126(R) (2020).
[28] C. Peng, L. Zhang, and Z.-Y. Lu, Phys. Rev. B **104**, 075112 (2021).
[29] J. Guo, J. Sun, X. Zhu, C.-A. Li, H. Guo, and S. Feng, J. Phys. Condens. Matter **34**, 035603 (2021).
[30] A. Hackenbroich, A. Hudomal, N. Schuch, B. A. Bernevig, and N. Regnault, Phys. Rev. B **103**, L161110 (2021).
[31] Y. Otsuka, T. Yoshida, K. Kudo, S. Yunoki, and Y. Hatsugai, Sci. Rep. **11**, 20270 (2021).
[32] D. González-Cuadra, Phys. Rev. B **105**, L020403 (2022).
[33] Y.-M. Li, Y.-J. Wu, X.-W. Luo, Y. Huang, and K. Chang, Phys. Rev. B **106**, 054403 (2022).
[34] A. Montorsi, U. Bhattacharya, D. González-Cuadra, M. Lewenstein, G. Palumbo, and L. Barbiero, Phys. Rev. B **106**, L241115 (2022).
[35] J. F. Wienand, F. Horn, M. Aidelsburger, J. Bibo, and F. Grusdt, Phys. Rev. Lett. **128**, 246602 (2022).
[36] S. V. Aksenov, A. D. Fedoseev, M. S. Shustin, and A. O. Zlotnikov, Phys. Rev. B **107**, 125401 (2023).
[37] W. P. Su, J. R. Schrieffer, and A. J. Heeger, Phys. Rev. Lett. **42**, 1698 (1979).
[38] R. E. Peierls, *Quantum Theory of Solids* (Oxford University Press, New York, 1955), Vol. 23.
[39] J. K. Asbóth, L. Oroszlány, and A. Pályi, Lect. Not. Phys. **919** (2016).
[40] A. J. Heeger, S. Kivelson, J. R. Schrieffer, and W. P. Su, Rev. Mod. Phys. **60**, 781 (1988).
[41] B. Xing, W.-T. Chiu, D. Poletti, R. T. Scalettar, and G. Batrouni, Phys. Rev. Lett. **126**, 017601 (2021).
[42] T. Chanda, R. Kraus, G. Morigi, and J. Zakrzewski, Quantum **5**, 501 (2021).
[43] D. Jaksch and P. Zoller, Ann. Phys. (Amsterdam) **315**, 52 (2005), special Issue.
[44] M. Lewenstein, A. Sanpera, V. Ahufinger, B. Damski, A. Sen(De), and U. Sen, Adv. Phys. **56**, 243 (2007).
[45] C. Gross and I. Bloch, Science **357**, 995 (2017).
[46] D. González-Cuadra, P. R. Grzybowski, A. Dauphin, and M. Lewenstein, Phys. Rev. Lett. **121**, 090402 (2018).
[47] H. Ritsch, P. Domokos, F. Brennecke, and T. Esslinger, Rev. Mod. Phys. **85**, 553 (2013).
[48] F. Mivehvar, F. Piazza, T. Donner, and H. Ritsch, Adv. Phys. **70**, 1 (2021).
[49] F. Mivehvar, H. Ritsch, and F. Piazza, Phys. Rev. Lett. **118**, 073602 (2017).
[50] D. González-Cuadra, A. Dauphin, P. R. Grzybowski, P. Wójcik, M. Lewenstein, and A. Bermudez, Phys. Rev. B **99**, 045139 (2019).
[51] D. González-Cuadra, A. Bermudez, P. R. Grzybowski, M. Lewenstein, and A. Dauphin, Nat. Commun. **10**, 2694 (2019).
[52] T. Chanda, R. Kraus, J. Zakrzewski, and G. Morigi, Phys. Rev. B **106**, 075137 (2022).
[53] T. Chanda, D. González-Cuadra, M. Lewenstein, L. Tagliacozzo, and J. Zakrzewski, SciPost Phys. **12**, 076 (2022).
[54] S. R. Manmana, A. M. Essin, R. M. Noack, and V. Gurarie, Phys. Rev. B **86**, 205119 (2012).
[55] J. Sirker, M. Maiti, N. P. Konstantinidis, and N. Sedlmayr, J. Stat. Mech. 10 (2014) P10032.
[56] D. Wang, S. Xu, Y. Wang, and C. Wu, Phys. Rev. B **91**, 115118 (2015).
[57] L. Barbiero, L. Santos, and N. Goldman, Phys. Rev. B **97**, 201115(R) (2018).
[58] B. Sbierski and C. Karrasch, Phys. Rev. B **98**, 165101 (2018).
[59] X.-L. Yu, L. Jiang, Y.-M. Quan, T. Wu, Y. Chen, L.-J. Zou, and J. Wu, Phys. Rev. B **101**, 045422 (2020).
[60] K. A. Fraser and F. Piazza, Commun. Phys. **2**, 48 (2019).
[61] D. González-Cuadra, A. Dauphin, P. R. Grzybowski, M. Lewenstein, and A. Bermudez, Phys. Rev. Lett. **125**, 265301 (2020).
[62] D. González-Cuadra, A. Dauphin, P. R. Grzybowski, M. Lewenstein, and A. Bermudez, Phys. Rev. B **102**, 245137 (2020).
[63] S. Julià-Farré, D. González-Cuadra, A. Patscheider, M. J. Mark, F. Ferlaino, M. Lewenstein, L. Barbiero, and A. Dauphin, Phys. Rev. Res. **4**, L032005 (2022).
[64] R. Landig, L. Hruby, N. Dogra, M. Landini, R. Mottl, T. Donner, and T. Esslinger, Nature (London) **532**, 476 (2016).
[65] J. Léonard, A. Morales, P. Zupancic, T. Esslinger, and T. Donner, Nature (London) **543**, 87 (2017).
[66] C. Maschler and H. Ritsch, Phys. Rev. Lett. **95**, 260401 (2005).

[67] D. Jaksch, C. Bruder, J. I. Cirac, C. W. Gardiner, and P. Zoller, Phys. Rev. Lett. **81**, 3108 (1998).
[68] See Supplemental Material at http://link.aps.org/supplemental/10.1103/PhysRevLett.131.263001 for the derivation of the effective Hamiltonian in Eqs. (1) and (2) and a study of the scaling of the order parameters with the bond dimension.
[69] S. R. White, Phys. Rev. Lett. **69**, 2863 (1992).
[70] J. Hauschild and F. Pollmann, SciPost Phys. Lect. Notes 5 (2018); code available from https://github.com/tenpy/tenpy.
[71] S.-S. Gong, W. Zhu, D. N. Sheng, O. I. Motrunich, and M. P. A. Fisher, Phys. Rev. Lett. **113**, 027201 (2014).
[72] L. Wang, Z.-C. Gu, F. Verstraete, and X.-G. Wen, Phys. Rev. B **94**, 075143 (2016).
[73] M. Mambrini, A. Läuchli, D. Poilblanc, and F. Mila, Phys. Rev. B **74**, 144422 (2006).
[74] F. Pollmann, A. M. Turner, E. Berg, and M. Oshikawa, Phys. Rev. B **81**, 064439 (2010).
[75] H. Araki, T. Mizoguchi, and Y. Hatsugai, Phys. Rev. Res. **2**, 012009(R) (2020).
[76] L. Lepori and L. Dell'Anna, New J. Phys. **19**, 103030 (2017).
[77] M. Atala, M. Aidelsburger, J. T. Barreiro, D. Abanin, T. Kitagawa, E. Demler, and I. Bloch, Nat. Phys. **9**, 795 (2013).
[78] M. Lohse, C. Schweizer, O. Zilberberg, M. Aidelsburger, and I. Bloch, Nat. Phys. **12**, 350 (2016).
[79] Y.-C. He, F. Grusdt, A. Kaufman, M. Greiner, and A. Vishwanath, Phys. Rev. B **96**, 201103(R) (2017).
[80] W. S. Bakr, J. I. Gillen, A. Peng, S. Fölling, and M. Greiner, Nature (London) **462**, 74 (2009).
[81] J. F. Sherson, C. Weitenberg, M. Endres, M. Cheneau, I. Bloch, and S. Kuhr, Nature (London) **467**, 68 (2010).
[82] C. Kokail, R. van Bijnen, A. Elben, B. Vermersch, and P. Zoller, Nat. Phys. **17**, 936 (2021).
[83] C. Kokail, B. Sundar, T. V. Zache, A. Elben, B. Vermersch, M. Dalmonte, R. van Bijnen, and P. Zoller, Phys. Rev. Lett. **127**, 170501 (2021).
[84] B. Wang, M. Aidelsburger, J. Dalibard, A. Eckardt, and N. Goldman, arXiv:2306.15610.